Received: 22 September 2019 | Revised: 4 January 2020 | Accepted: 9 February 2020

DOI: 10.1002/we.2494

RESEARCH ARTICLE

WILEY

Prediction of seismic loadings on wind turbine support structures by response spectrum method considering equivalent modal damping of support structures and reliability level

Masaru Kitahara | Takeshi Ishihara

Department of Civil Engineering, School of Engineering, The University of Tokyo, Tokyo, Japan

Correspondence
Takeshi Ishihara, Department of Civil Engineering, School of Engineering, The University of Tokyo, 7-3-1, Hongo, Bunkyo-ku, Tokyo, Japan.
Email: ishihara@bridge.t.u-tokyo.ac.jp

Funding information
Shimizu Corporation, Hitachi Ltd, ClassNK

Abstract

In this study, a new damping correction factor is proposed to provide an accurate design response spectrum for megawatt (MW) class wind turbines. The predicted response spectra show good agreement with those by time history analysis (THA). An equivalent modal damping of wind turbine support structures is then proposed for response spectrum method (RSM) based on the modal decomposition method for non-classically damped structures. Seismic loadings on wind turbine towers and footings by RSM with the proposed damping correction factor and equivalent modal damping are also investigated and compared with those by THA. Finally, a quantile value between 0.5 and 0.85 in the damping correction factor is calibrated to ensure the same reliability level as evaluated by THA currently used for estimation of seismic loadings on support structures.

KEYWORDS

damping correction factor, equivalent modal damping, reliability level, response spectrum method, seismic loading, wind turbine support structure

1 | INTRODUCTION

In recent years, the expansion in wind energy has increased the construction of wind turbines in seismically active regions requiring a simple and accurate procedure for estimation of seismic loadings on wind turbine support structures. A wind turbine piled foundation was damaged at Kashima Wind farm during Great East Japan Earthquake (11 March 2011),[1] and a wind turbine tower was buckled during Kumamoto Earthquake (16 April 2016).[2] The structural integrity of wind turbine support structures during such extreme events should be investigated by the reliable design.

Time history analysis (THA) takes into account the impact of higher modes to seismic responses and is widely used for estimation of seismic loadings on wind turbines under both the parked and the operational conditions by Witcher,[3] Kjørlaug et al,[4] Prowell et al,[5] Asareh et al,[6] Avossa et al,[7] Failla et al,[8] and Zuo et al.[9] However, the results by THA vary largely depending on input acceleration time histories, which requires a large number of analyses for reliable seismic loading estimation. In case of the large wind farm consisting of dozens of wind turbines, a convenient and precise estimation procedure is desired.

On the other hand, it is also possible to consider the contribution from higher modes to seismic loadings by response spectrum method (RSM). A study was conducted for estimation of seismic loadings on wind turbine towers by RSM with the complete quadratic combination (CQC)

The peer review history for this article is available at https://publons.com/publon/10.1002/we.2494.

rule considering up to the third mode of towers by Ishihara and Sawar.[10] However, due to the low structural damping ratio of wind turbines, acceleration response spectra have an excessive fluctuation, and it is not possible to consider the fluctuation by conventional damping correction factors in Eurocode,[11] and the Building Standard Law in Japan.[12] Damping correction factors with a quantile value taking into account the uncertainty in response spectra were proposed for different damping ratio ranges; one was for the damping ratio between 0.5% and 5% by Ishihara et al,[13] and the other was for the damping ratio larger than 5% by Ishihara and Takei.[14] However, the structural damping ratio of a 2.4 MW wind turbine is around 0.2% as mentioned by Oh and Ishihara[15]; hence, a damping correction factor for megawatt (MW) class wind turbines needs to be investigated.

Moreover, RSM requires modal damping ratios of support structures, while there are no mentions about how to estimate them in the previous studies as well as in International Electrotechnical Commission (IEC) 61400-1 Annex D.[16] Although modal damping ratios can be calculated by complex eigenvalue analysis, it may cause prediction errors because damped modal shapes are generally different from undamped modal shapes, which are used in RSM with the CQC rule. RSM based on damped modal shapes was also proposed by Igusa et al,[17] however this method may also cause prediction errors due to empirical assumptions in the modal participation factor and modal combination rule.

In this study, a new damping correction factor is proposed for MW class wind turbines, and an equivalent modal damping for wind turbine support structures is then proposed based on the modified modal decomposition method for non-classically damped structures. Seismic loadings on a 2-MW wind turbine tower and footing by RSM with the proposed damping correction factor and equivalent modal damping are also investigated for two typical soil conditions and compared with those by THA. The accuracy of the proposed method is further systematically verified by case studies with different tower geometries and different soil conditions. Finally, a quantile value between 0.5 and 0.85 in the damping correction factor is calibrated to ensure the same reliability level as evaluated by THA currently used for estimation of seismic loadings on support structures in Japan Society of Civil Engineers (JSCE).[18]

2 | MODELS AND METHODS FOR SEISMIC LOADING ESTIMATION

The outline of a 2-MW wind turbine and its support structures, their numerical models, and two typical soil models used in this study are described in Section 2.1. The overview of the acceleration response spectrum and RSM with the CQC rule is then shown in Sections 2.2 and 2.3. The validation metric to quantify the accuracy of the proposed method is also presented in Section 2.4.

2.1 | Model descriptions

Figure 1 shows sway-rocking (SR) model which is widely used for estimation of seismic loadings on wind turbine support structures considering soil-structure interaction (SSI).[18-21] Here, *z* and *x* express the vertical and horizontal axes. The first, second and *n*th nodes represent the footing, tower base, and hub height, respectively. In SR model, the tower is modeled as a multi degree of freedom (MDOF) system. Figure 1A shows a standard lumped mass (SLM) model, which includes the detail configuration of the rotor and nacelle, used for the design of wind turbines. On the other hand, Figure 1B illustrates an approximated lumped mass (ALM) model used in this study, which simplifies rotor and nacelle assembly (RNA) as a lumped mass at the hub height and is employed for estimation of seismic loadings on support structures. The footing mass and ground are connected by the sway and rocking springs and dashpots to consider SSI. Note that the frequency dependence of the springs and dashpots, the cross-coupling between the sway and rocking springs, and the mass moment of inertia of foundations are neglected in SR model for the simplification.

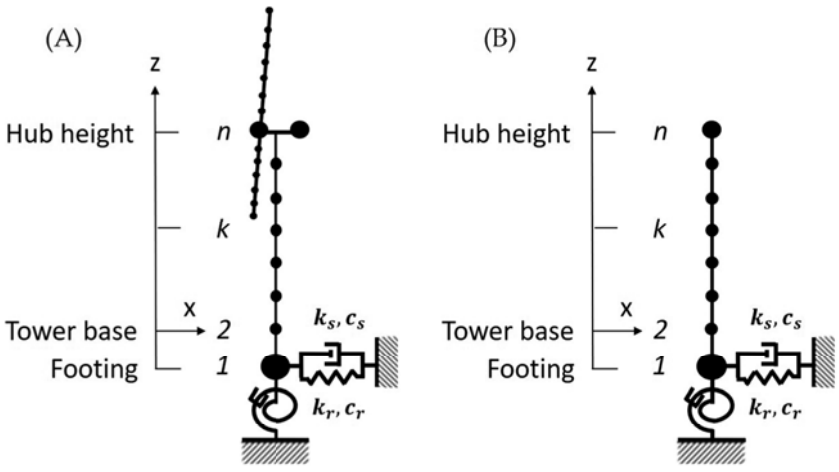

FIGURE 1 Sway-rocking model for wind turbine support structures: (A) standard lumped mass model and (B) approximate lumped mass model

TABLE 1 Outline of a 2-MW wind turbine and its support structures

Item	Description
Rotor diameter (m)	83
Tower height (m)	67
Rotor and nacelle mass (kg)	112 000
Tower mass (kg)	165 100
Tower top diameter (m)	2.34
Tower top thickness (mm)	13
Tower bottom diameter (m)	4.23
Tower bottom thickness (mm)	35
Structural damping ratio of the first mode (%)	0.2
Structural damping ratio of the second mode (%)	0.2
Footing width (m)	16
Footing depth (m)	3
Footing mass (kg)	1 551 170
Pile diameter (m)	1.5
Pile distance (m)	6.5
Number of piles in the x-direction	3
Number of piles in the y-direction	3
Total number of piles	8
Young modulus of the pile (kN/m^2)	22 800 000
Density of the concrete (kg/m^3)	2446.5
The gravity foundation for the soil type I	
Stiffness constant in the sway direction k_s (N/m)	8.56×10^9
Stiffness constant in the rocking direction k_r (Nm/rad)	5.74×10^{11}
Damping coefficient in the sway direction c_s (Nsec/m)	2.07×10^7
Damping coefficient in the rocking direction c_r (Nmsec/rad)	7.04×10^8
The piled foundation for the soil type II	
Stiffness constant in the sway direction k_s (N/m)	7.90×10^8
Stiffness constant in the rocking direction k_r (Nm/rad)	4.03×10^{11}
Damping coefficient in the sway direction c_s (Nsec/m)	3.02×10^7
Damping coefficient in the rocking direction c_r (Nmsec/rad)	1.02×10^9

Table 1 shows the outline of a 2-MW wind turbine and its support structures used in this study. The structural damping ratio of the first mode is estimated using the formula proposed by Oh and Ishihara.[15] The same value as the first mode is also used for the second mode and Rayleigh damping model is used to calculate structural damping ratios of higher modes as recommended in JSCE.[18] The footing mass is about six times the total masses of the tower, rotor, and nacelle, which is the general case in seismically active regions like Japan.[18] In addition, a slightly embedded footing with the embedment ratio, which is defined as the ratio of the footing depth to width, is assumed as 0.2 and ensures that the representation of SSI by the uncoupled sway and rocking springs and dashpots is a reasonable simplification.

A gravity foundation is used for the soil type I (the stiff soil condition), and a piled foundation is used for the soil type II (the soft soil condition). For the gravity foundation, stiffness constants of the springs and damping coefficients of the dashpots are estimated by the cone model as shown in Architectural Institute of Japan (AIJ).[22] On the other hand, for the piled foundation, stiffness constants of the sway and rocking springs are calculated by Francis and Randolph models, respectively,[23,24] and damping coefficients of the dashpots are obtained from Gazetas model.[25] The detailed derivation of the springs and dashpots was shown by Ishihara and Wang.[21] In addition, the calculation of these properties requires equivalent S-wave velocities and damping coefficients of one-dimensional layered soil models, and they are calculated based on a method by Okano and Sako,[26] briefly introduced in Section 2.2.

Table 2 shows the description of one-dimensional layered soil models for the soil type I and soil type II used in this study as shown in AIJ.[22] Note that even for the soil type II, shear strain is less than 1%, and the equivalent linearization method is applicable.

TABLE 2 Description of one-dimensional layered soil models

Layer No.	Depth (m)	Density (t/m^3)	S-wave Velocity (m/s)	P-wave Velocity (m/s)	Soil Type
(a) Soil type I					
1	3	1.7	130	320	Sand
2	5.7	1.8	340	720	Sand
3	10	1.7	280	720	Clay
4	17.4	1.9	380	1980	Sand
Bedrock	–	2.1	510	1980	Rock
(b) Soil type II					
1	4.5	1.8	90	1360	Clay
2	10	1.6	150	1560	Sand
3	17	1.8	210	1560	Sand
4	18.5	1.7	150	1560	Clay
5	25	1.8	260	1560	Sand
Bedrock	–	1.8	400	1700	Rock

2.2 | Acceleration response spectrum

For accurate estimation of seismic loadings on wind turbine support structures, the acceleration response spectrum considering the soil amplification factor and damping correction factor is required. The acceleration response spectrum is a function of the natural period T and damping ratio ζ of single degree of freedom (SDOF) system. The acceleration response spectrum used in this study is the following equation as recommended in Eurocode,[11] the Building Standard Law of Japan,[12] and American Society of Civil Engineers (ASCE)[27]:

$$S_a(T,\zeta) = \begin{cases} a_0 G_s \left\{ 1 + (F_\zeta \beta_0 - 1)\dfrac{T}{T_B} \right\} & (0 \le T < T_B) \\ a_0 G_s F_\zeta \beta_0 & (T_B \le T < T_C) \\ a_0 G_s F_\zeta \beta_0 \left(\dfrac{T_C}{T} \right) & (T_C \le T < T_D) \\ a_0 G_s F_\zeta \beta_0 \left(\dfrac{T_C}{T_D} \right)^{K_1} \left(\dfrac{T_D}{T} \right)^{K_2} & (T_D \le T), \end{cases} \tag{1}$$

where a_0 is the peak ground acceleration at the bedrock condition, G_s is the soil amplification factor, F_ζ is the damping correction factor, β_0 is the acceleration response magnification ratio for the region where acceleration responses become constant, and T_B, T_C, T_D, K_1, and K_2 are coefficients representing the shape of the response spectrum. The return period of the peak ground acceleration is defined as 475 years in IEC61400-1.[16] Parameters used for defining the target acceleration response spectrum for input acceleration time histories used in this study are listed in Table 3 based on the Building Standard Law in Japan.[12]

The target response spectrum for input acceleration time histories is generally defined at the bedrock condition considering the damping ratio as 5%; hence, the soil amplification should be considered to estimate acceleration response spectra at the footing base. A method for evaluating the soil amplification based on the framework of RSM using the one-dimensional wave propagation theory was proposed by Okano and Sako.[26]

Figure 2 illustrates acceleration response spectra with the damping ratio of 5.0% at the footing base for both the soil type I and soil type II by Okano and Sako,[26] along with the target response spectrum at the bedrock condition. Plots in the figure also show the mean value of response spectra obtained by THA of SDOF system using 15 input acceleration time histories at the footing base obtained by SHAKE.[28] The input acceleration time histories for SHAKE are defined at the bedrock condition with the same target response spectrum but have different phase properties. Four acceleration time histories, namely, El Centro NS,[29] Taft NS,[29] Hachinohe EW,[29] and JMAKobe EW,[30] show typical phase properties of observed earthquakes and 11 acceleration time histories have random phase properties. Acceleration response spectra by Okano and Sako[26]

TABLE 3 Parameters of the target acceleration response spectrum

a_0 (m/s^2)	β_0	K_1	K_2	T_B (s)	T_C (s)	T_D (s)
3.2	2.5	1	1	0.16	0.64	3.0

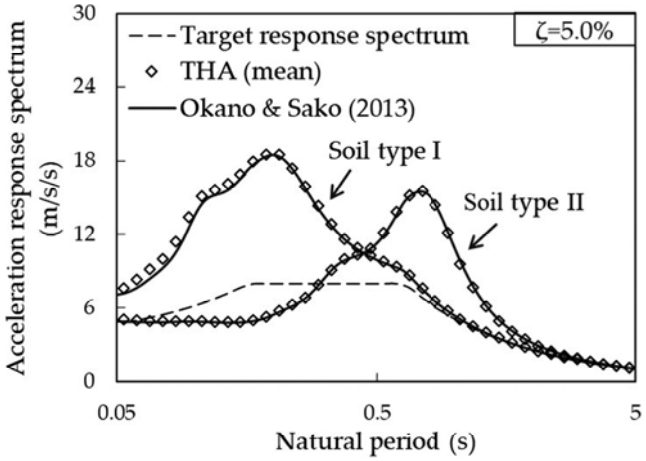

FIGURE 2 Acceleration response spectra at the footing base

show good agreement with those by THA and are used for RSM in this study. On the other hand, above 15 seismic acceleration time histories at the footing base are used for THA in Sections 3.3 and 3.4.

Moreover, acceleration response spectra severely depend on the damping ratio. The response spectra in Figure 2 are defined as the damping ratio, 5.0%. Nevertheless, the structural damping ratio of wind turbines are quite lower than 5%; thus, it is also important to consider the damping correction factor for accurate estimation of seismic loadings on wind turbine support structures. Furthermore, the damping correction factor is required to capture the fluctuation in response spectra and this issue is further discussed in Section 3.1.

2.3 | Response spectrum method

The equation of motion of wind turbine support structures' *j*th mode can be represented as

$$\ddot{q}_j + 2\zeta_j\omega_j\dot{q}_j + \omega_j^2 q_j = -\beta_j\ddot{u}_g, \tag{2}$$

where q_j, ζ_j, ω_j, and β_j are the modal displacement, modal damping ratio, natural frequency, and modal participation factor of the *j*th mode, respectively, and $\ddot{u}_g$ is the input acceleration time history. The modal participation factor β_j is expressed by Equation (3):

$$\beta_j = \frac{X_j^T \boldsymbol{m}\{e\}}{X_j^T \boldsymbol{m} X_j}, \tag{3}$$

where X_j is the undamped modal shape of the *j*th mode, $\boldsymbol{m}$ is the mass matrix, and $\{e\}$ is the unit vector. Note that only modal shapes in the sway direction are considered in RSM and those in the rocking direction are neglected.

The maximum acceleration, displacement, and force in the sway direction of the *j*th mode at the *k*th node can be estimated by Equations (4) to (6), respectively:

$$A_{kj} = \beta_j X_{kj} S_a(T_j, \zeta_j), \tag{4}$$

$$D_{kj} = \beta_j X_{kj} S_a(T_j, \zeta_j)\left(\frac{T_j}{2\pi}\right)^2, \tag{5}$$

$$F_{kj} = \beta_j X_{kj} S_a(T_j, \zeta_j) m_k, \tag{6}$$

where X_{kj} is the undamped modal shape of the *j*th mode at the *k*th node, $S_a(T_j, \zeta_j)$ is the acceleration response spectrum of the *j*th mode at the footing base, corresponding to its natural period T_j and modal damping ratio ζ_j, and m_k is the *k*th nodal mass. The maximum acceleration, displacement, shear force, and bending moment on support structures are then obtained by Equations (7) to (10), respectively:

$$A_k = \sqrt{\sum_{j=1}^{m} A_{kj}^2}, \text{with } A_{kj}^2 = \sum_{l=1}^{m} \rho_{jl} A_{kj} A_{kl}, \tag{7}$$

$$D_k = \sqrt{\sum_{j=1}^{m} D_{kj}^2}, \text{with } D_{kj}^2 = \sum_{l=1}^{m} \rho_{jl} D_{kj} D_{kl}, \tag{8}$$

$$Q_k = \sqrt{\sum_{j=1}^{m} Q_{kj}^2}, \text{with } Q_{kj}^2 = \sum_{l=1}^{m} \rho_{jl} \left[\sum_{k=i}^{n} F_{kj}\right] \left[\sum_{k=i}^{n} F_{kl}\right], \tag{9}$$

$$M_k = \sqrt{\sum_{j=1}^{m} M_{kj}^2}, \text{with } M_{kj}^2 = \sum_{l=1}^{m} \rho_{jl} \left[\sum_{k=i}^{n} F_{kj}(z_n - z_k)\right] \left[\sum_{k=i}^{n} F_{kl}(z_n - z_k)\right], \tag{10}$$

where m and n are the highest mode and node considered for calculations, z_n and z_k are the nth and kth nodal heights, and ρ_{jl} is the correlation coefficient between the jth and lth modes obtained by Equation (11) based on the CQC rule[31]:

$$\rho_{jl} = \frac{8\sqrt{\zeta_j \zeta_l}\left(\zeta_j + r_{jl}\zeta_l\right) r_{jl}^{3/2}}{\left(1 - r_{jl}^2\right)^2 + 4\zeta_j \zeta_l r_{jl}\left(1 + r_{jl}^2\right) + 4\left(\zeta_j^2 + \zeta_l^2\right) r_{jl}^2}, \tag{11}$$

where $r_{jl} = \omega_l / \omega_j$ is the natural frequency ratio of the jth to lth modes.

2.4 | Validation metric

In order to quantify the agreement between the results by THA and the proposed method, a hit rate q is introduced as the validation metric (see Schatzmann et al[32] and Oettl[33]) and is defined by Equation (12):

$$q = \frac{1}{N}\sum_{i=1}^{N} n_i, \text{with } n_i = \begin{cases} 1, & \left|\frac{y_i - x_i}{x_i}\right| \le D_q \\ 0, & else \end{cases}, \tag{12}$$

where x_i and y_i are the values by THA and the proposed method for the ith case, respectively, N is the total number of cases, and D_q is the threshold. Values of the metric corresponding to the complete agreement and disagreement are $q = 1$ and $q = 0$, respectively. Following the German Verein Deutscher Ingenieure (VDI) guideline 3783-9,[34] a threshold $D_q = 0.25$ is used in this study as suggested by Schatzmann et al[32] and Oettl.[33]

3 | SEISMIC LOADING ESTIMATION FOR WIND TURBINE SUPPORT STRUCTURES

Acceleration response spectra of the damping ratio, 0.2%, are investigated, and a new damping correction factor is proposed for MW class wind turbines in Section 3.1. The identification of an equivalent modal damping for RSM with the CQC rule is also presented in Section 3.2. Seismic loadings on the 2-MW wind turbine tower and footing by RSM with the proposed damping correction factor and equivalent modal damping are then investigated and compared with those by THA in Section 3.3. The accuracy of the proposed method is further verified by case studies with different tower geometries and different soil conditions in the same section. A quantile value between 0.5 and 0.85 in the damping correction factor is finally calibrated in Section 3.4 to ensure the same reliability level as evaluated by THA currently used for estimation of seismic loadings on support structures in JSCE.[18]

3.1 | A new damping correction factor for MW class wind turbines

Due to the low structural damping ratio of wind turbines, capturing the fluctuation in acceleration response spectra by the damping correction factor is significant. Acceleration response spectra with damping ratios 5.0% and 0.2% are investigated by THA of SDOF system using the 15 acceleration time histories defined at the bedrock condition (same as the input acceleration time histories for SHAKE in Section 2.2). Figure 3 shows mean values of the results by the 15 acceleration time histories, and error bars indicate their standard deviations. It can be seen that the

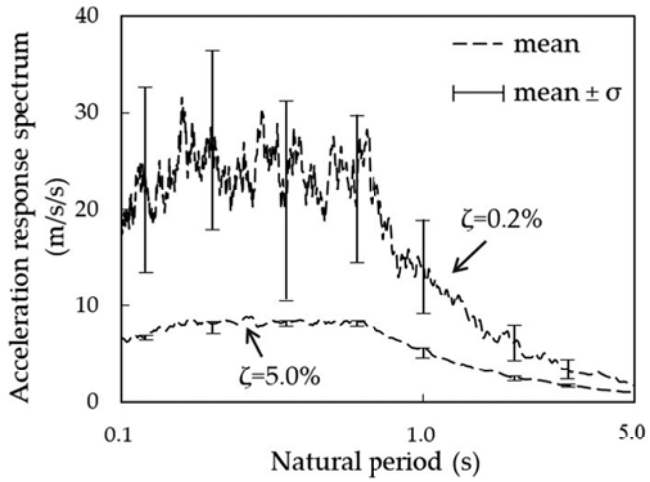

FIGURE 3 Acceleration response spectra with damping ratios 5.0% and 0.2%

mean value of response spectra with the damping ratio 0.2% is larger than that with the damping ratio 5.0% and the standard deviation of response spectra with the damping ratio 0.2% is quite large while that with the damping ratio 5.0% can be negligible.

The cumulative distribution function of acceleration responses, which represents the uncertainty in acceleration response spectra, is calculated dividing response spectra into three sections based on Equation (1), so that $0.1 \le T < T_B$ refers to the section I_A, $T_B \le T < T_C$ refers to the section I_B, and $T_C \le T < 5$ refers to the section I_C. Sections I_A and I_C that define nonlinear regions of the design response spectrum are still divided into 10 subsections $I_A^{(i)}$ and $I_C^{(i)}$ (i = 1~10), whereas the section I_B is considered as a single section. Percentile values of acceleration responses are then calculated from the cumulative distribution function. In this study, a damping correction factor for the damping ratio less than 5.0% is defined as Equation (13):

$$F_\zeta(\zeta, T, \gamma) = \left(\frac{5.2}{0.2 + 100\zeta}\right)^{\alpha}, \text{with}\, \alpha = f(T, \gamma), \tag{13}$$

where γ is the quantile value. Note that $F_\zeta(\zeta, T, \gamma)$ will be one when ζ = 5% to obtain the acceleration response spectrum at the bedrock condition. Figure 4 illustrates a relationship between the natural period, quantile value, and α in Equation (13) obtained by THA. Equation (14) shown in the figure is estimated by the least square method as

$$\alpha = -0.05T + 0.35\gamma + 0.3. \tag{14}$$

Figure 5 shows a comparison of acceleration response spectra of the damping ratio, 0.2% calculated by THA and the proposed formula for quantile values, γ = 0.2, 0.5, and 0.8. Acceleration response spectra using the proposed damping correction factor match well with those by THA

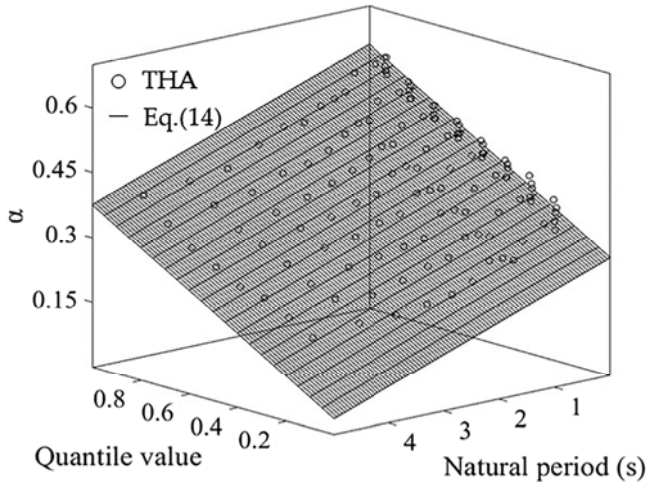

FIGURE 4 Relationship between the natural period, quantile value, and α

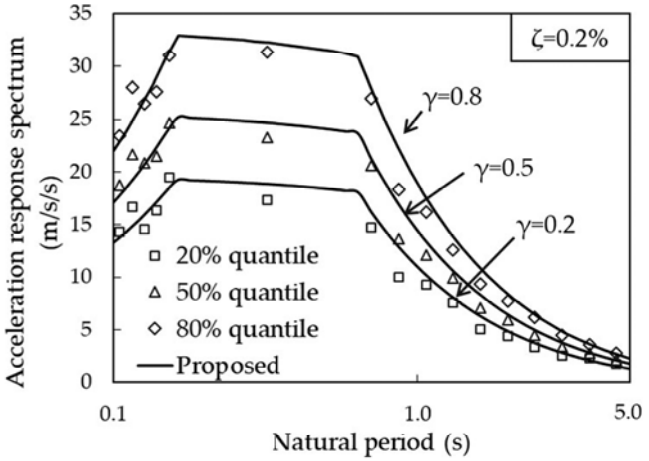

FIGURE 5 Comparison of acceleration response spectra by time history analysis (THA) and the proposed formula

for all quantile values. The introduction of the natural period to the damping correction factor leads to accurate estimation of response spectra especially in long-period regions and the uncertainty in response spectra can be incorporated by changing the quantile value.

Finally, the damping correction factor used in this study is summarized in Equation (15) with the formula for the damping ratio lager than 5% proposed by Ishihara and Takei.[14]

$$F_\zeta = \begin{cases} \left(\dfrac{5.2}{0.2+100\zeta}\right)^{-0.05T+0.35\gamma+0.3} & (\zeta < 0.05) \\ \left(\dfrac{2}{-3+100\zeta}\right)^{0.15\log_{10}\frac{T}{1.5\gamma}+0.3} & (\zeta > 0.05) \end{cases}. \tag{15}$$

Figure 6 shows a comparison of the damping correction factor in Eurocode,[11] the previous formula by Ishihara and Takei,[14] and Equation (15) with the results by THA. The natural period is set as the second modal natural period of the 2-MW wind turbine on the soil type I as shown in Table 4 (T = 0.33 s). This mode has the largest contribution to the shear force on towers as shown in Figure 11A. A quantile value is also fixed as γ = 0.5. It is found that the damping correction factor is significantly underestimated by the formula in Eurocode,[11] and the previous formula by Ishihara and Takei,[14] especially for the lower damping ratio range, while the proposed formula agrees well with that by THA for the whole damping ratio range.

3.2 | Identification of an equivalent modal damping

RSM with the CQC rule requires modal damping ratios of undamped modes. They can be identified as an equivalent modal damping of support structures comparing each modal maximum shear force by damped and undamped modal shapes of towers based on the modified modal decomposition method for non-classically damped structures (see Appendix A).

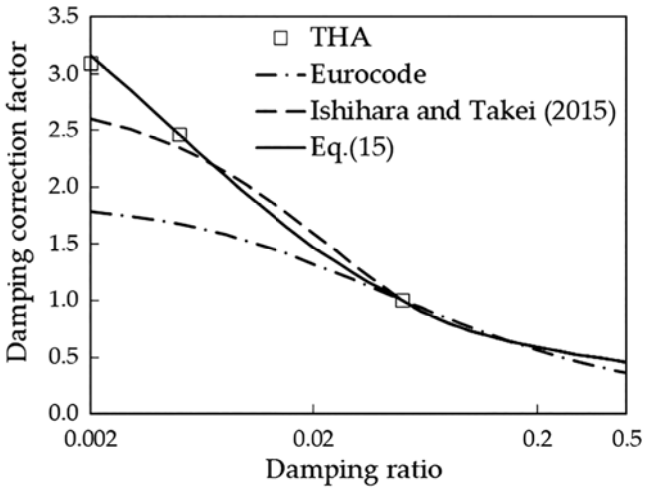

FIGURE 6 Comparison of various damping correction factors

TABLE 4 Comparison of damped and undamped modal properties

Mode	ζ_{damped} (%)	T_{damped} (s)	ζ_{eq} (%)	$T_{undamped}$ (s)
(a) Soil type I				
1	0.2	2.477	0.20	2.477
2	0.2	0.331	0.21	0.331
3	0.8	0.113	0.83	0.113
4	8.5	0.085	5.00	0.085
5	1.1	0.058	1.03	0.058
(b) Soil type II				
1	0.2	2.478	0.21	2.478
2	1.5	0.333	5.00	0.342
3	40.8	0.283	5.00	0.275
4	0.8	0.112	0.10	0.112
5	1.1	0.058	0.10	0.058

Modal damping ratios of damped modes are calculated by complex eigenvalue analysis. Complex eigenvalue analysis solves the equation as

$$\begin{bmatrix} \boldsymbol{m} & \boldsymbol{0} \\ \boldsymbol{0} & -\boldsymbol{k} \end{bmatrix} \Psi_j = \lambda_j \begin{bmatrix} \boldsymbol{0} & \boldsymbol{m} \\ \boldsymbol{m} & \boldsymbol{c} \end{bmatrix} \Psi_j, \tag{16}$$

where $\boldsymbol{m}$, $\boldsymbol{c}$, and $\boldsymbol{k}$ are the mass, damping, and stiffness matrices, respectively, and Ψ_j and λ_j are the complex eigenvector and complex eigenvalue of the jth mode. The eigenvector Ψ_j and eigenvalue λ_j are in complex-conjugate pairs. The modal damping ratio of damped modes is then obtained as

$$\zeta_{damped} = -\mathrm{Re}(\lambda_j)/|\lambda_j|, \tag{17}$$

and the eigenvector Ψ_j is explained as

$$\Psi_j = \begin{bmatrix} \lambda_j \phi_j \\ \phi_j \end{bmatrix}, \tag{18}$$

where ϕ_j is the damped modal shape of the jth mode. The damped modal shape ϕ_j is also in complex-conjugate pairs and is generally different from the undamped modal shape X_j as shown in Equation (3). For the special case where structures are classically damped, ϕ_j is real-valued and coincides with X_j.

The calibration rule to identify the equivalent modal damping is summarized here. Each modal maximum shear force on towers Q_{kj} (k = 2~n) is estimated by Equation (A8) using modal damping ratios of damped modes and their modal shapes. Modal damping ratios of undamped modes are then increased from an initial value of 0.1%, and corresponding modal maximum shear forces Q_{kj} are calculated by Equation (9) to find modal damping ratios which provide the minimum square error between Q_{kj} by Equation (A8) and Equation (9). As mentioned in Appendix A, the maximum shear force corresponding to the sway motion of foundations might be underestimated due to the large modal damping ratio of this mode. Although this mode has few contributions to the shear force on towers, it has a large contribution to the shear force on footings. In this study, the maximum modal damping ratio is selected as 5.0% to prevent the underestimation of the shear force on footings by the proposed method. The identified modal damping ratios are considered as the equivalent modal damping of support structures in this study. Note that the modal participation factor as Equation (A11) is used for estimation of Q_{kj} by Equation (A8).

Table 4 shows a comparison between modal damping ratios of damped modes ζ_{damped} as Equation (17) and equivalent modal damping ratios ζ_{eq} of the 2-MW wind turbine, with natural periods of damped modes T_{damped} and undamped modes $T_{undamped}$. Figures 7 and 8 show vertical profiles of the real part of damped modal participation functions $\gamma_j\phi_j$ and undamped modal participation functions $\beta_j X_j$. On the soil type I, the equivalent modal damping ratios are almost same as the modal damping ratios of damped modes because the natural periods of undamped modes are equal to those of damped modes and the undamped modal participation functions agree well with the real part of the damped modal participation functions.

More attention is paid for the results on the soil type II, where the equivalent modal damping ratios of the second and third modes are significantly different from the modal damping ratios of corresponding damped modes, while the natural periods of undamped modes

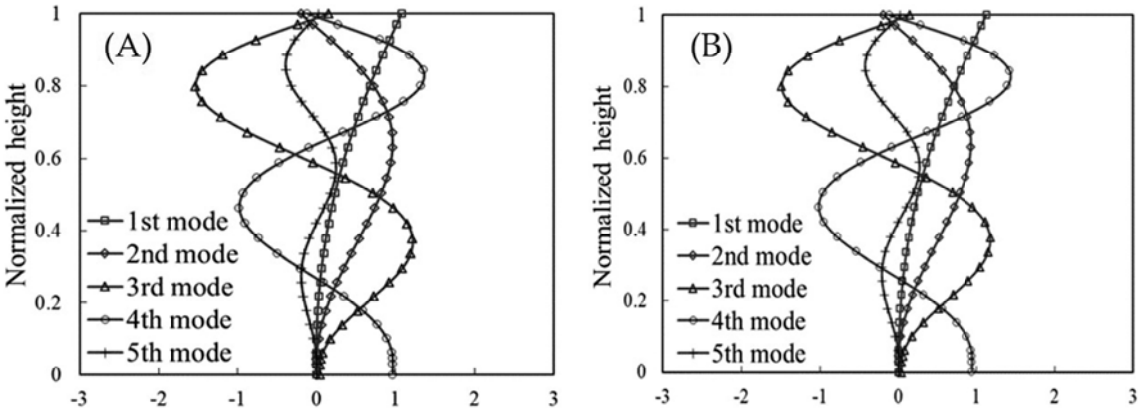

FIGURE 7 Modal participation functions on the soil type I: (A) real part of damped modes and (B) undamped modes

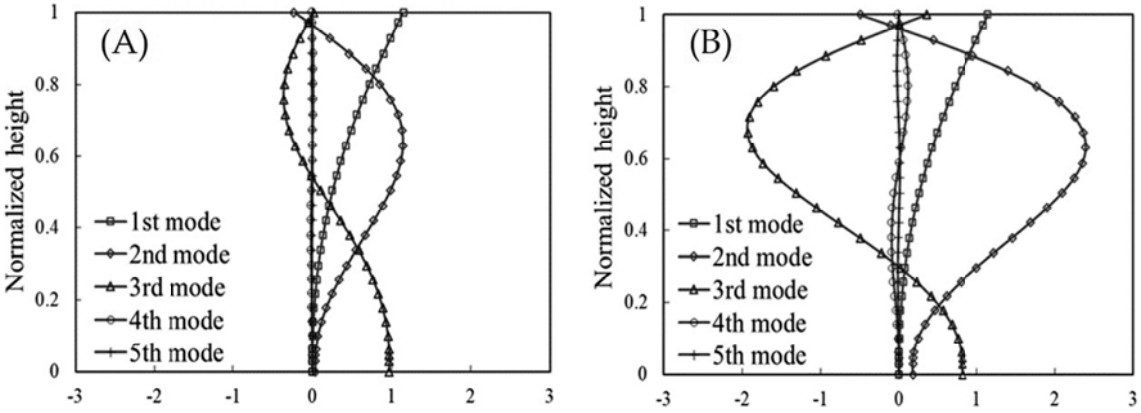

FIGURE 8 Modal participation functions on the soil type II: (A) real part of damped modes and (B) undamped modes

are almost same as those of damped modes. These discrepancies are caused by the difference between the undamped modal participation functions and the real part of the damped modal participation functions of those modes. The second damped mode has fewer contributions from the sway motion of foundations than the second undamped mode. Hence, the corresponding equivalent modal damping ratio is larger than the modal damping ratio of the damped mode. On the other hand, the third damped mode has much larger contributions from the sway motion of foundations than the third undamped mode; thus, the corresponding equivalent modal damping ratio is smaller than the modal damping ratio of the damped mode.

3.3 | Seismic loading estimation by the proposed method

Seismic loadings on the 2-MW wind turbine tower and footing are estimated by RSM with the proposed damping correction factor and equivalent modal damping. In this study, it is determined to consider up to the fifth mode to satisfy the criteria of model code for concrete chimneys.[35] THA by the SLM and ALM models, shown in Figure 1, is also performed using a developed finite element method (FEM) program,[36] to validate the results by the proposed method.

Figure 9 plots a comparison of the shear force and bending moment profiles on the tower by the proposed method with a quantile value $\gamma = 0.5$ in the damping correction factor and mean values obtained by THA using the 15 acceleration time histories as mentioned in Section 2.2. THA by the SLM and ALM models gives almost the same loadings, while the shear force by the ALM model are slightly overestimated on the soil type I since the shear force contributed from the second mode is slightly overestimated due to the quite small damping ratio of the second mode, as shown in Table 4. Hence, only the ALM model is considered in the rest part for estimating seismic loadings on towers. In addition, the bending moments at the hub height by the ALM model without consideration of the mass moment of inertia of RNA are underestimated, whereas they can be considered as an additional loading by RNA. In this study, the additional loading by P $-$ Δ effect is also considered, and these two additional loadings are expressed as

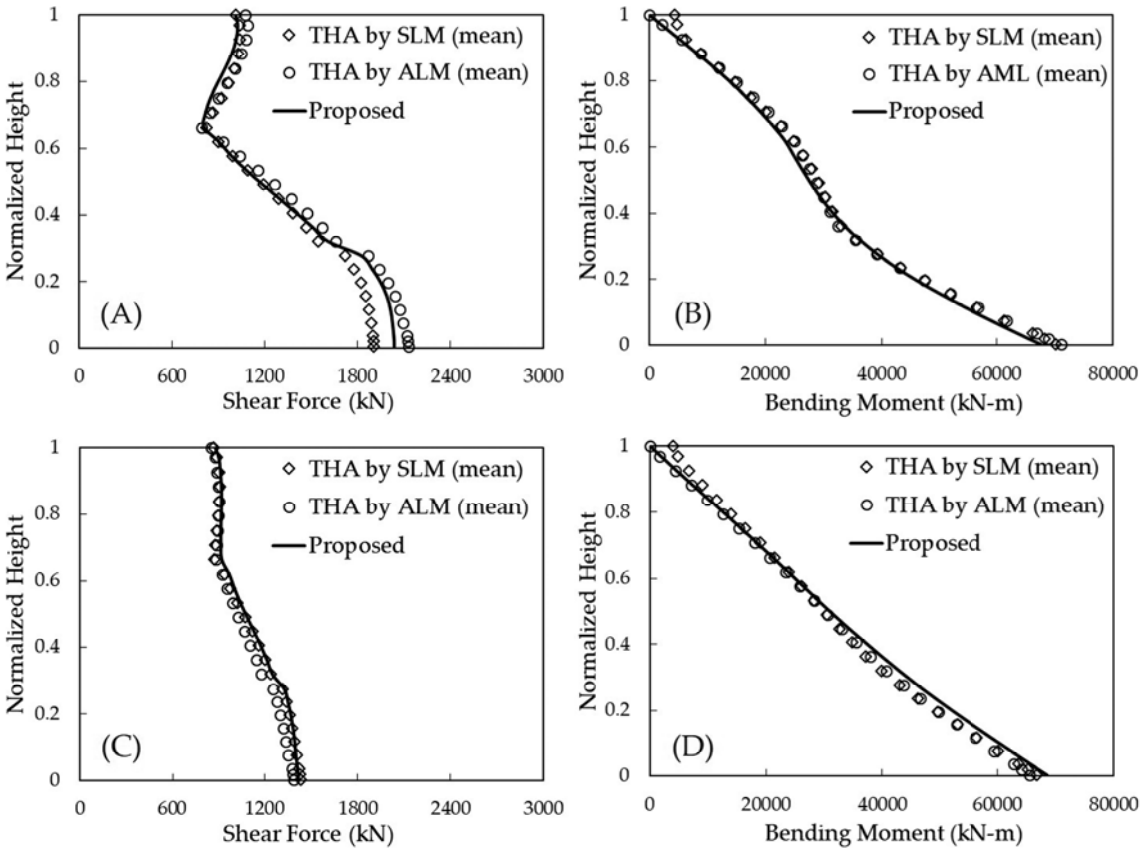

FIGURE 9 Vertical profiles of seismic loadings on the tower: (A) Shear force on the soil type I, (B) bending moment on the soil type I, (C) shear force on the soil type II, and (D) bending moment on the soil type II

$$M_k^{RNA} = C \times I_y \times \ddot{\theta} \times \left(\frac{z_k}{z_n}\right)^5 = C \times I_y \times \frac{A_{n,1} - A_{n-1,1}}{z_n - z_{n-1}} \times \left(\frac{z_k}{z_n}\right)^5, C = 0.5, \tag{19}$$

$$M_k^{PD} = \sum_{j=k+1}^{N} m_k g (D_j - D_k), \tag{20}$$

where M_k^{RNA} and M_k^{PD} are bending moments by the mass moment of inertia of RNA and P – Δ effect both at the kth node, respectively, I_y is the mass moment of inertia of RNA, $\ddot{\theta}$ is the angular acceleration at the hub height, $A_{n,1}$ is the maximum acceleration of the first mode at the nth node calculated by Equation (4), z_n and z_k are the nth and kth nodal heights, and C is a correction factor. In addition, m_k is the kth nodal mass, g is the gravitational acceleration, and D_k is the maximum displacement at the kth node estimated by Equation (8). Table 5 lists the angular velocity of RNA at the hub height, additional moments by RNA at the hub height, and P – Δ effect at the tower base. The numbers in parentheses show the ratio of these additional moments to the bending moment at the tower base. Note that differences between the predicted additional moments of RNA by the SLM model and those by Equation (19), as shown in Table 5, are less than 1%.

More attention is paid for the results by the proposed method, which show good agreement with the mean values obtained from THA by the ALM model; thus, the equivalent modal damping ratios calibrated in Section 3.2 are validated as modal damping ratios of undamped modes.

TABLE 5 Additional loadings by rotor and nacelle assembly (RNA) and P – Δ effect for different soil types

	RNA		P – Δ Effect
	ω (rad/s)	M_n^{RNA} (kN-m)	M_1^{PD} (kN-m)
Soil type I	0.075	2974 (4.2%)	1313 (1.8%)
Soil type II	0.077	3537 (5.0%)	1538 (2.2%)

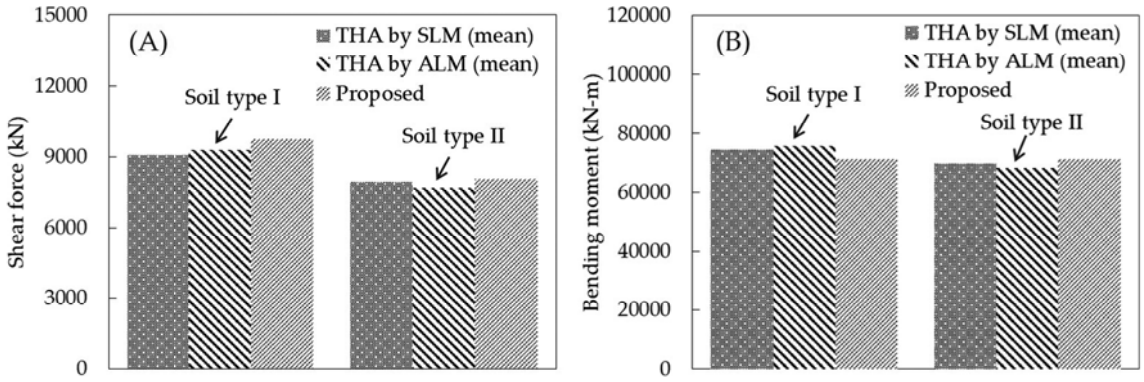

FIGURE 10 Seismic loadings acting on the footing: (A) shear forces and (B) bending moments

TABLE 6 Prediction bias error (percentage) for different soil types

	Shear force		Bending Moment	
	Tower base	Footing	Tower base	Footing
Soil type I (%)	−4.34	4.76	−4.95	−6.04
Soil type II (%)	2.30	5.03	4.53	4.11

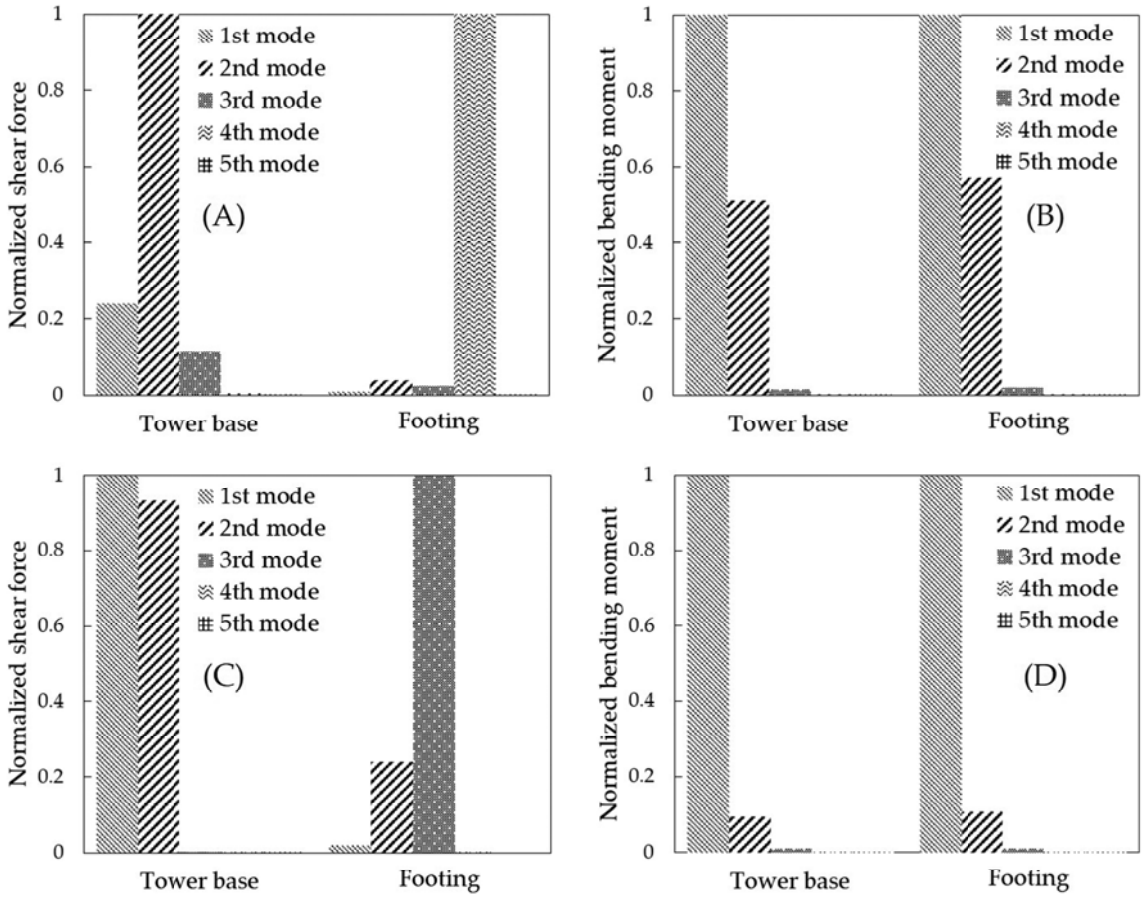

FIGURE 11 Contribution of each mode to seismic loadings at the tower base and footing: (A) shear force on the soil type I, (B) bending moment on the soil type I, (C) shear force on the soil type II, and (D) bending moment on the soil type II

TABLE 7 Description of wind turbine models with different rated powers

Item	Description					
Rated power (kW)	**500**	**1000**	**1500**	**2000**	**2500**	**3000**
Rotor diameter (m)	40	56	72	83	92	95
Tower height (m)	40	56	60	67	72	75
Rotor mass (kg)	5800	17 200	28 400	34 000	36 500	38 000
Nacelle mass (kg)	12 000	43 000	61 000	78 000	94 000	98 700
Tower mass (kg)	27 000	90 300	107 500	165 100	179 000	187 200
Turbine total mass (kg)	44 800	1 505 000	196 900	277 100	309 500	323 900
Footing width (m)	9	13	14	16	16	16
Footing depth (m)	1.5	2	2.5	3	3	3
Footing mass (kg)	245 399.9	813 422.3	989 678.8	1 551 170	1 551 170	1 551 170
Mass ratio	0.183	0.185	0.199	0.179	0.200	0.209
Natural period of first mode (s)	1.307	2.072	2.105	2.477	2.649	2.694
Damping ratio of first mode (%)	0.516	0.285	0.280	0.230	0.214	0.210

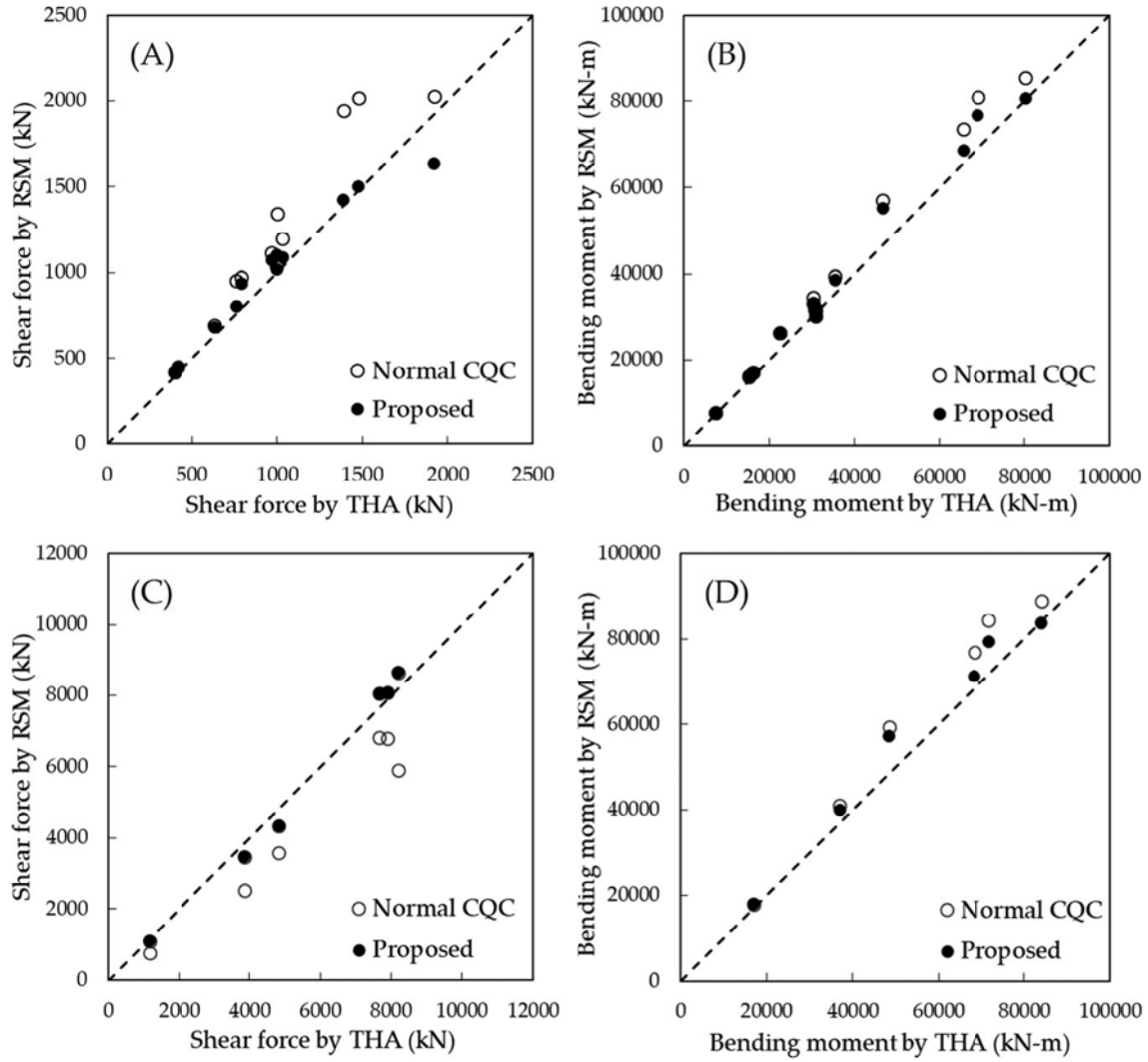

FIGURE 12 Comparison of predicted seismic responses by the normal complete quadratic combination (CQC) and proposed methods with those by time history analysis (THA) for different tower geometries: (A) shear forces on towers, (B) bending moments on towers, (C) shear forces on footings, and (D) bending moments on footings

Figure 10 illustrates a comparison of the shear force and bending moment acting on the footing by the proposed method with a quantile value γ = 0.5 and mean values calculated by THA using the 15 acceleration time histories. THA by both models gives almost the same results; thus, only the ALM model is used in the rest part for estimation of seismic loadings on footings. Moreover, the results by the proposed method are in good agreement with the mean values obtained from THA by the ALM model. It should be noticed that the equivalent modal damping is estimated to make seismic responses on towers by undamped modes close to those by damped modes and seismic responses on footings are not considered anymore. However, the sway mode of footings is consecutively connected with that of towers and it supposes to lead reasonable estimation of seismic loadings on footings based on the identified equivalent modal damping.

Table 6 lists the prediction bias error (percentage) in the shear force and bending moment at the tower base and footing by RSM with the proposed damping correction factor and equivalent modal damping comparing with mean values of THA results by the ALM model. It is found that the accuracy of the predicted seismic loadings by the proposed method is quite well, especially for the shear force on the footing which is quite important for designing piled foundations, and the predicted bias error is within 10% for both the tower base and footing irrespective of the soil type.

Figure 11 shows a contribution of each mode to the shear force and bending moment at the tower base and footing. It reveals that considering up to the third mode is enough to estimate the shear force and bending moment on towers irrespective of the soil type and, in particular, the first mode is dominant for the bending moment as mentioned by Ishihara and Sawar.[10] On the other hand, the sway motion of foundations, such as the fourth mode on the soil type I and the third mode on the soil type II, is dominant for the shear force on footings, while the first mode is still dominant for the bending moment on footings.

Finally, the prediction accuracy of the proposed method is further systematically verified by case studies with different tower geometries and different soil conditions.

Six wind turbines with the rated power of 500, 1000, 1500, 2000, 2500, and 3000 kW supported by the piled foundation on the soil type II are built based on Xu and Ishihara.[37] Stiffness constants of the sway and rocking springs are calculated by Francis and Randolph models, respectively,[23,24] and damping coefficients of the sway and rocking dashpots are obtained from Gazetas model,[25] for each wind turbine model. Table 7 describes these wind turbine models. The natural period of the first mode is obtained by eigenvalue analysis, and the corresponding structural damping ratio is calculated by Equation (21) as proposed by Oh and Ishihara[15]:

$$\zeta_{struc\,1}(\%) = 2.0e^{-1.3T_1} + 0.15, \tag{21}$$

where ζ_{struc1} and T_1 is the structural damping ratio and natural period of the first mode.

Figure 12 shows a comparison of shear forces and bending moments at the 1/2 height, tower base, and footing by the normal CQC and proposed methods with mean values of those by THA using the 15 acceleration time histories. A quantile value γ = 0.5 in the damping correction factor is considered for both the normal CQC and proposed methods. The normal CQC method indicates RSM with the CQC rule directly accounting

TABLE 8 Validation metrics for the results by the normal complete quadratic combination (CQC) and proposed methods

	Tower		Footing	
Model	Shear force	Bending moment	Shear force	Bending moment
Normal CQC	0.75	1.00	0.33	1.00
Proposed	1.00	1.00	1.00	1.00

TABLE 9 Stiffness constants and damping coefficients with different equivalent S-wave velocities

Item	Description					
V_{se} (m/s)	100	150	200	250	300	350
Stiffness constant in the sway direction k_s (N/m)	6.79×10^8	1.55×10^9	2.76×10^9	4.22×10^9	5.90×10^9	7.77×10^9
Stiffness constant in the rocking direction k_r (Nm/rad)	6.81×10^{10}	1.76×10^{11}	3.31×10^{11}	5.05×10^{11}	6.76×10^{11}	8.39×10^{11}
Damping coefficient in the sway direction c_s (Nsec/m)	3.97×10^7	3.30×10^9	2.56×10^7	1.96×10^7	1.55×10^7	1.37×10^7
Damping coefficient in the rocking direction c_r (Nmsec/rad)	4.04×10^8	5.08×10^8	6.06×10^8	6.68×10^8	7.01×10^8	7.18×10^8

for modal damping ratios by complex eigenvalue analysis. It can be seen that the predicted shear forces and bending moments on towers and footings by the proposed method show favorable agreement with those by THA.

On the other hand, the normal CQC method tends to overestimate the shear forces on towers as shown in Figure 12A. The sway motion of foundations appears on both the second and third undamped modes on the soil type II, while it appears on only the third damped mode, as shown in Figure 8, for the 2-MW turbine. The shear forces on towers are overestimated by the normal CQC method since the second modal damping ratio by complex eigenvalue analysis is smaller than the corresponding equivalent modal damping ratio. As shown in Table 4 (b), the second modal damping ratio by complex eigenvalue analysis is 1.5%, while the equivalent modal damping ratio is estimated as 5.0%. The normal CQC method also tends to underestimate the shear forces on footings because the third modal damping ratio by complex eigenvalue analysis is much larger than the corresponding equivalent modal damping ratio, as shown in Table 4 (b), in which the third modal damping ratio by complex eigenvalue analysis is 40.8%, while the equivalent modal damping ratio is estimated as 5.0%. As explained in Appendix A, the third modal maximum shear force by Equation (A8) might be underestimated, thus that by Equation (9) with the equivalent modal damping ratio also might be underestimated. Although the predicted shear forces on footings by the proposed method are slightly underestimated, the errors are within an acceptable range.

Table 8 lists the validation metrics by Equation (12) for the results by the normal CQC and proposed methods. It is found that the proposed method shows good performance for all cases, especially for the shear forces on footings which are important for the design of piled foundations. On the other hand, whereas the normal CQC method also presents good performance for the bending moments, hit rates for the shear forces are not allowable (in particular, the hit rate on footings is less than 40%).

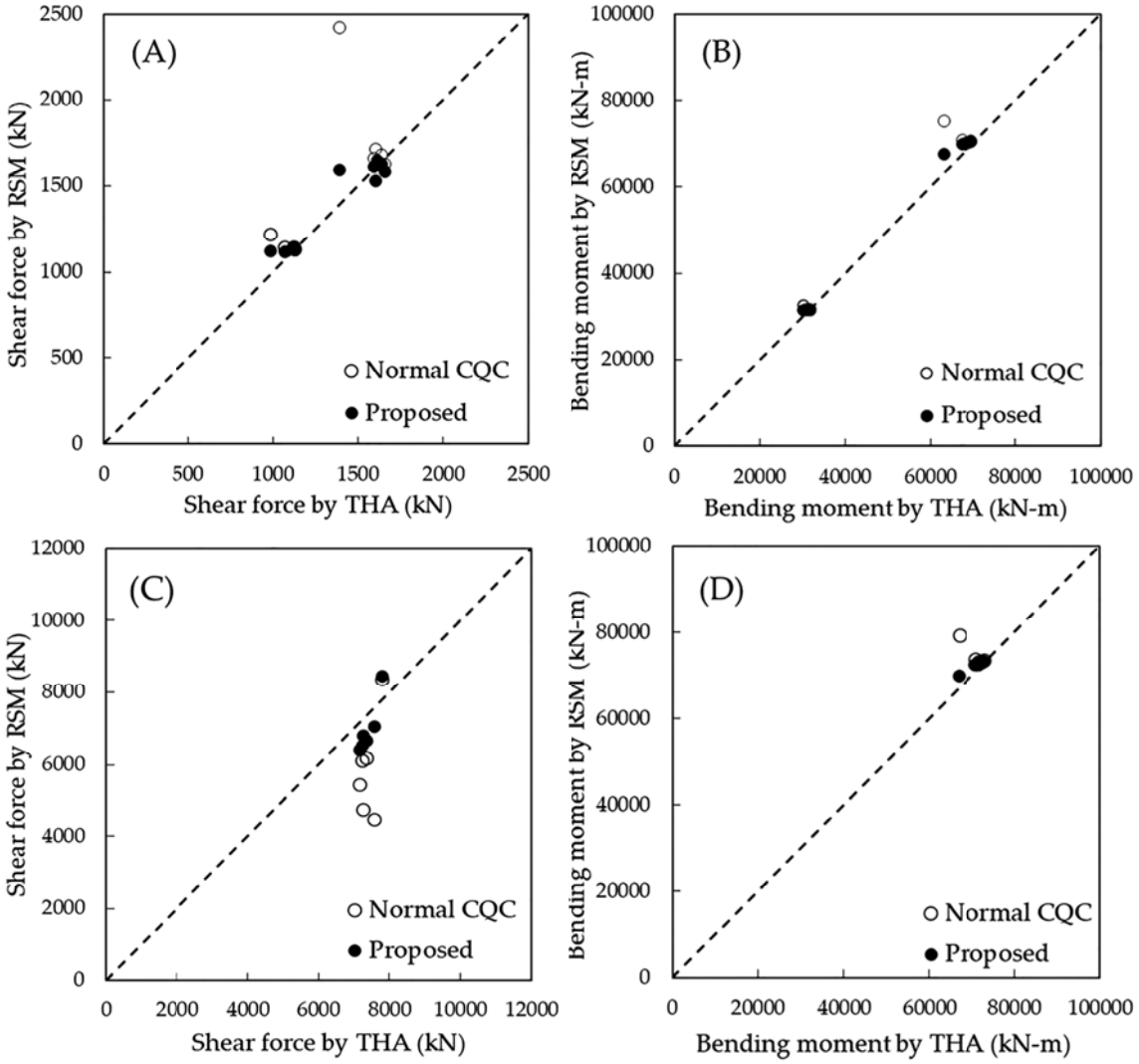

FIGURE 13 Comparison of predicted seismic responses by the normal complete quadratic combination (CQC) and proposed methods with those by time history analysis (THA) for different soil conditions: (A) shear forces on towers, (B) bending moments on towers, (C) shear forces on footings, and (D) bending moments on footings

Six soil models with the equivalent S-wave velocity of 100, 150, 200, 250, 300, and 350 m/s are considered, and stiffness constants of the sway and rocking springs and damping coefficients of the sway and rocking dashpots are calculated for the 2-MW wind turbine, as described in Table 1. The equivalent S-wave velocity is calculated as Equation (22) based on the cone model shown in AIJ[22]:

$$V_{se} = \sqrt{G_e/\rho_1},\ G_e = \beta_h G_1, \tag{22}$$

here,

$$\beta_h = \frac{1}{\sum\left(\frac{1}{\alpha_i}\right)}, \alpha_i = \left(\frac{G_i}{G_1}\right)\frac{(z_i z_{i-1})}{z_0(z_i - z_{i-1})}, \alpha_n = \left(\frac{G_n}{G_1}\right)\frac{z_{n-1}}{z_0}, z_0 = \pi r_0 \frac{2-\nu_i}{8},\ z_i = z_0 + \sum h_i, \tag{23}$$

where G_i, ν_i, ρ_i, and h_i are the complex shear modulus, Poisson ratio, soil density, and thickness of the ith layer, respectively, and r_0 is the equivalent radius of the foundation bottom. The equivalent S-wave velocity of the soil type II based on above equations is 139.8 m/s. Table 9 summarizes stiffness constants of the springs calculated by Francis and Randolph models[23,24] and damping coefficients of the dashpots obtained by Gazetas models[25] for each soil model.

Figure 13 shows a comparison of shear forces and bending moments at the 1/2 height, tower base, and footing by the normal CQC and proposed methods with mean values of those by THA using the 15 acceleration time histories. A quantile value γ = 0.5 in the damping correction

TABLE 10 Validation metrics for the results by the normal complete quadratic combination (CQC) and proposed methods

	Tower		Footing	
Model	Shear force	Bending moment	Shear force	Bending moment
Normal CQC	0.92	1.00	0.67	1.00
Proposed	1.00	1.00	1.00	1.00

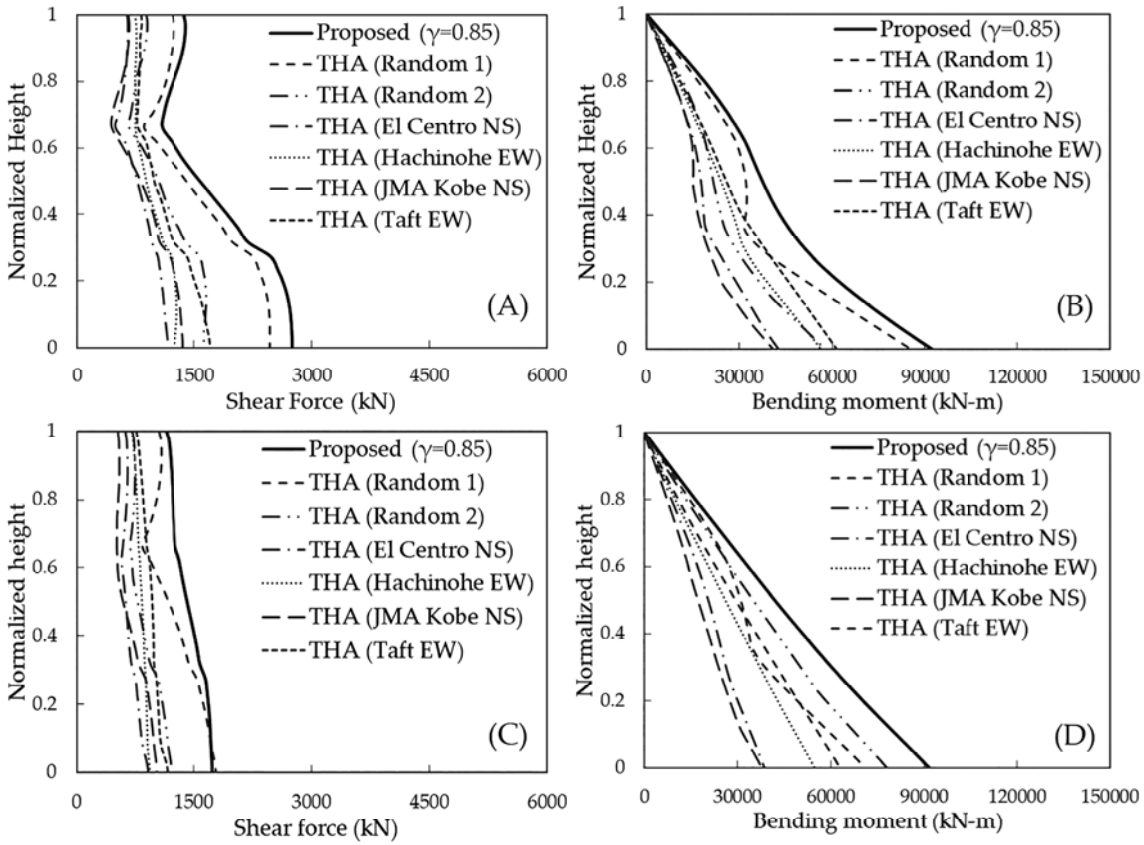

FIGURE 14 Vertical profiles of seismic loadings on the tower for different acceleration time histories: (A) shear force on the soil type I, (B) bending moment on the soil type I, (C) shear force on the soil type II, and (D) bending moment on the soil type II

factor is considered for both the normal CQC and proposed methods. The predicted shear forces and bending moments on towers and footings by the proposed method show favorable agreement with those by THA.

On the other hand, the normal CQC method significantly overestimates the shear forces on towers for the case with the equivalent S-wave velocity of 100 m/s. The normal CQC method also tends to underestimate shear forces on footings regardless of the soil condition due to the large modal damping ratio calculated by complex eigenvalue analysis. Although the proposed method also slightly underestimates shear forces on footings, the errors are within an allowable range.

Table 10 details the validation metrics by Equation (12) for the results by the normal CQC and proposed methods. It is found that the proposed method shows favorable performance for all of the cases, including the shear forces on footings. On the other hand, although the normal CQC method also provides good hit rates in most cases, the hit rate for the shear forces on footings is less than 70% and not allowable.

3.4 | Reliability level of seismic loadings

In the last section, the proposed method is compared with the mean values of THA; thus, a quantile value γ = 0.5 is considered in the damping correction factor. On the other hand, the quantile value accounts for the uncertainty in acceleration response spectra, as mentioned in Section 3.1, and it is essential to determine a suitable quantile value for describing the reliable design response spectrum. In IEC 61400-1 Annex D, it is mentioned that a quantile value between 0.5 and 0.85 can be used considering the local requirement.[16] For example, the maximum value of THA using at least six acceleration time histories with different phase properties is required in JSCE.[18] Hence, a quantile value needs to be calibrated to give the same reliability level as the corresponding value of THA.

Firstly, a suitable quantile value for defining the design response spectrum, which coincides with the maximum values of THA using the six acceleration time histories, is calibrated based on a comparison between seismic loadings on the 2-MW wind turbine support structures by the proposed method and THA. Two local earthquakes, Hachinohe EW[29] and JMA Kobe NS,[30] and two famous earthquakes, El Centro NS[29] and Taft EW,[29] are used as phase properties of input acceleration time histories, and two random phase acceleration time histories are also considered. All acceleration time histories are generated at the footing base.

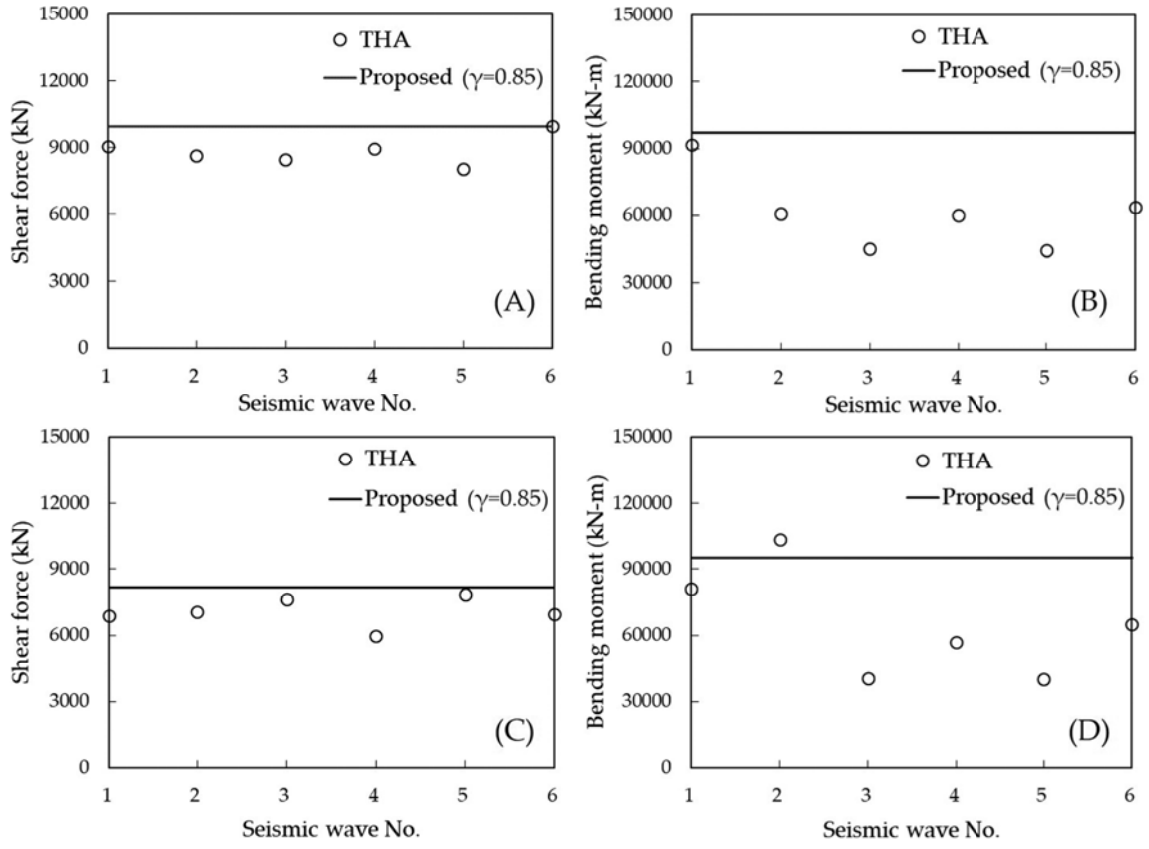

FIGURE 15 Seismic loadings acting on the footing for different acceleration time histories (1: Random 1, 2: Random 2, 3: El Centro NS, 4: Hachinohe EW, 5: JMA Kobe NS, 6: Taft EW): (A) shear force on the soil type I, (B) bending moment on the soil type I, (C) shear force on the soil type II, and (D) bending moment on the soil type II

Figure 14 illustrates shear forces and bending moments on the tower by the proposed method with a quantile value γ = 0.85 in the damping correction factor and the results by THA using the six acceleration time histories. Seismic loadings on the tower by THA show large uncertainties due to differences in the phase property of the acceleration time histories. Moreover, the results by the proposed method with the quantile value γ = 0.85 almost correspond to the maximum values by THA; thus, the quantile value γ = 0.85 can be used to describe the design response spectrum for support structures with the same reliability level as the current design code in JSCE.[18]

Figure 15 plots shear forces and bending moments on the footing by the proposed method with a quantile value γ = 0.85 and THA using the six acceleration time histories. It is found that shear forces on the footing have a few sensitivities to the phase property of acceleration time histories, while bending moments on the footing still have large uncertainties. The predicted values by the proposed method with the quantile value γ = 0.85 almost correspond to the maximum values by THA, especially for shear forces on the footing which are important for designing piled foundations. Hence, the quantile value γ = 0.85 can be also used to derive the design response spectrum for foundations ensuring the same reliability level as evaluated by THA in JSCE.[18]

Finally, the proposed method with a quantile value between 0.5 and 0.85 is demonstrated to obtain seismic loadings on the support structures and foundations, and they are compared with corresponding quantile values by THA to validate the quantile value in IEC 61400-1 Annex D.[16] Figures 16 shows shear forces and bending moments at the tower base and footing by the proposed method with the quantile value between 0.5 and 0.85 in the damping correction factor. Cumulative mass functions of shear forces and bending moments by THA using the 15 acceleration time histories are also plotted in the figure. Seismic loadings by the proposed method with the quantile value between 0.5 and 0.85 show favorable agreement with the corresponding cumulative relative frequency between 0.5 and 0.85 derived by THA. Hence, the proposed method can analytically calculate seismic loadings on wind turbine support structures with the desired reliability level using the quantile value between 0.5 and 0.85 in the new damping correction factor, and its accuracy is same as the corresponding quantile value by THA used in current design codes.[11,18]

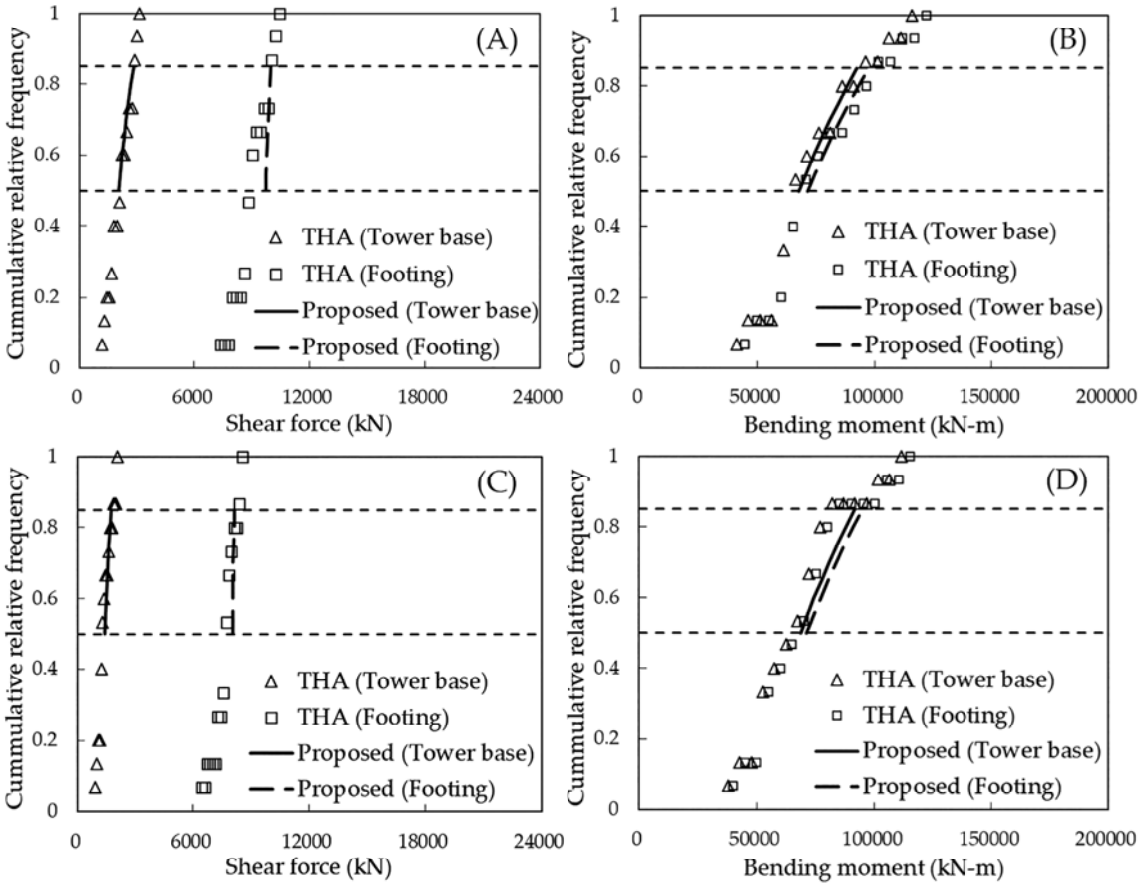

FIGURE 16 Seismic loadings at the tower base and footing corresponding to the reliability level: (A) shear forces on the soil type I, (B) bending moments on the soil type I, (C) shear forces on the soil type II, and (D) Bending moments on the soil type II

4 | CONCLUSION

In this study, a new damping correction factor is proposed to provide an accurate acceleration response spectrum for MW class wind turbines. An equivalent modal damping of wind turbine support structures for RSM is then investigated to predict seismic loadings on support structures. A quantile value in the new damping correction factor is also introduced, and seismic loadings on towers and footings are estimated corresponding to the reliability level. Conclusions and some recommendations on the use of the proposed RSM for estimation of seismic loadings on wind turbine support structures are summarized below.

1. A new damping correction factor is proposed to consider excessive fluctuations in acceleration response spectra, and the accuracy of acceleration response spectra for MW class wind turbines with the low structural damping ratio is improved.
2. An equivalent modal damping for RSM is proposed based on the modified modal decomposition method for non-classically damped structures. Seismic loadings on wind turbine towers and footings by RSM with the proposed damping correction factor and equivalent modal damping show favorable agreement with those by THA, while the normal CQC method overestimates or underestimates seismic loadings.
3. A quantile value between 0.5 and 0.85 in the damping correction factor is validated by THA. Seismic loadings on wind turbine support structures by the proposed method with a suitable quantile value show the same reliability level as those by THA used in current design codes.
4. Bending moments on towers used for designing towers are governed by lower modes of towers and can be estimated using the modal damping by complex eigenvalue analysis, while shear forces on footings required for designing piled foundations have large contributions from higher modes, such as the sway motion of foundations, and the proposed equivalent modal damping needs to be employed.

ACKNOWLEDGEMENTS

This research was carried out as a part of the project funded by Shimizu Corporation, Hitachi Ltd., and ClassNK. The authors express their deepest gratitude to the concerned parties for their assistance during this study.

ORCID

Masaru Kitahara https://orcid.org/0000-0001-9877-9574

REFERENCES

1. Ashford SA, Boulanger RW, Donahue JL, Stewart JP. Geotechnical quick report in the Kanto plain region during the March 11, 2011, Off Pacific Coast of Tohoku Earthquake, Japan. GEER Association Report No. GEER-025a, 2011.
2. Harukigaoka Wind Power Inc. A prompt report on No.2 wind turbine tower damage in Kugino Wind Farm. 2016. (In Japanese) http://www.meti.go.jp/shingikai/sankoshin/hoan_shohi/denryoku_anzen/newenergy_hatsuden_wg/pdf/009_05_00.pdf.
3. Witcher D. Seismic analysis of wind turbines in the time domain. *Wind Energy*. 2005;8:81-91.
4. Kjørlaug RA, Kaynia AM, Elgamal A. Seismic response of wind turbines due to earthquake and wind loading. *Proc EURODYN*. 2014;3627-3634.
5. Prowell I, Elgamal A, Uang CM, Luco JE, Romanowitz H, Duggan E. Shake table testing and numerical simulation of a utility-scale wind turbine including operational effects. *Wind Energy*. 2014;17:997-1016.
6. Asareh MA, Schonberg W, Volz J. Effects of seismic and aerodynamic load interaction on structural dynamic response of multi-megawatt utility scale horizontal axis wind turbines. *Renew Energy*. 2016;86:49-58.
7. Avossa AM, Demartino C, Ricciardelli F. Assessment of the peak response of a 5MW HAWT under combined wind and seismic induced loads. *Open Construct Build Technol J*. 2017;11:441-457.
8. Failla G, Santangelo F, Foti G, Arena F, Scali F. Response-spectrum uncoupled analysis for seismic assessment of offshore wind turbines. *J Mar Sci Eng*. 2018;6(3):1-24.
9. Zuo H, Bi K, Hao H, Li C. Influence of earthquake ground motion modelling on the dynamic responses of offshore wind turbines. *Soil Dyn Earthq Eng*. 2019;121:151-167.
10. Ishihara T, Sawar MW. Numerical and theoretical study on seismic response of wind turbines. *Proc EWEC*. 2008;1-5.
11. Eurocode 8, Design of Structures for Earthquake Resistance - Part 1: General Rules, Seismic Actions and Rules for Buildings, EN-1998-1, 2004.
12. The Building Standard Law of Japan. The building centre of Japan, 2004.
13. Ishihara T, Takamoto G, Sarwar MW. Seismic load evaluation of wind turbine support structures with consideration of uncertainty in response spectrum and higher modes. *Proc OFFSHORE*. 2011;1-9.
14. Ishihara T, Takei Y. Seismic load estimation of wind turbine support structure considering a new damping correction factor for response spectrum method. *J JWEA*. 2015;39:14-22. (In Japanese)
15. Oh S, Ishihara T. Structural parameter identification of a 2.4 MW bottom fixed wind turbine by excitaion test using active mass damper. *Wind Energy*. 2018;21(11):1232-1238.
16. International Electrotechnical Commission 61400-1. 4th Wind turbine generator systems Part1, Safety requirements. International Electrotechnical Commission, 2019.
17. Igusa T, Kasai K, Yamashita T. Effects of non-classical damping in passively controlled structures. International Symposium on Earthquake Engineering Commemorating Tenth Anniversary of the 1995 Kobe earthquake, 2005:227–236.
18. Ishihara T. (Ed). Guidelines for design of wind turbine support structure and foundations. Japanse Society of Civil Engineers, 2010. (In Japanese).
19. ISO 3010, Bases for design of structures—Seismic actions on structures. International Organization for Standardization, 2001.

20. Butt UA, Ishihara T. Seismic load evaluation of wind turbine support structures considering low structural damping and soil structure interaction. *Proc EWEA*. 2012;1-9.
21. Ishihara T, Wang L. A study of modal damping for offshore wind turbines considering soil properties and foundation types. *Wind Energy*. 2019;22(12): 1760-1778.
22. Architectural Institute of Japan. Seismic response analysis and design of buildings considering dynamic soil-structure interaction. 2006. (In Japanese).
23. Francis AJ. Analysis of pile groups with flexural resistance. *J Soil Mech Found Div*. 1964;90:1-32.
24. Randolph MF. The response of flexible piles to lateral loading. *Géotechnique*. 1981;31(2):247-259.
25. Gazetas G, Dobry R. Horizontal response of piles in layered soils. *J Geotech Engrg*. 1984;110:20-40.
26. Okano H, Sako Y. Proposal of evaluation method for amplification of response spectrum by surface strata. *J Technol Design*. 2013;19:47-52. (In Japanese)
27. American Society of Civil Engineers 7-05. Minimum design loads for buildings and other structures. American Society of Civil Engineers, 2006.
28. Schnabel PB, Lysmer J, Seed HB. SHAKE a computer program for earthquake response analysis of horizontal layered sites. Report No EERC72–12, University of California, Berkeley, 1972.
29. Building Performance Standardization Association. Typical observed seismic waves (acceleration data). (In Japanese) http://www.seinokyo.jp/jsh/top/.
30. Japan Meteorological Agency. Strong seismic waveform (the 1995 Southern Hyogo Prefecture Earthquake). (In Japanese). http://www.data.jma.go.jp/svd/cqcv/data/kyoshin/jishin/hyogo_nanbu/index.html.
31. Kiureghian AD. A response spectrum method for random vibration analysis of mdf systems. *Earthquake Eng Struct Dyn*. 1981;9(5):419-435.
32. Schatzmann M, Olesen H, Franke J. (Eds). COST 732 model evaluation case studies: approach and results. *COST Office Brussels*. 2010.
33. Oettl D. Quality assurance of the prognostic, microscale wind-field model GRAL 14.8 using wind-tunnel data provided by the German VDI guideline 3783–9. *J Wind Eng Ind Aerodyn*. 2015;142:104-110.
34. The German Verein Deutscher Ingenieure guideline 3783-9. Environmental meteorology—Prognostic microscale wind field models—Evaluation for flow around buildings and obstacles. *Tech Rep VDI guideline*. 2005.
35. CICIND. Model code for concrete chimneys, Part A: The shell, 2010.
36. Ishihara T, Phuc PV, Fujino Y, Takahara K, Mekaru T. A field test and full dynamic simulation on a stall regulated wind turbine. *Proc of APCWE*. 2005;6: 599-612.
37. Xu N, Ishihara T. Analytical formulae for wind turbine tower loading in the parked condition by using quasi-steady analysis. *Wind Eng*. 2014;38(3): 291-309.
38. Zhou XY, Yu RF, Dong D. Complex mode superposition algorithm for seismic responses of non-classically damped linear MDOF system. *J Earthq Eng*. 2004;8:597-641.

How to cite this article: Kitahara M, Ishihara T. Prediction of seismic loadings on wind turbine support structures by response spectrum method considering equivalent modal damping of support structures and reliability level. *Wind Energy*. 2020;1–22. https://doi.org/10.1002/we.2494

APPENDIX A: Modified modal decomposition method for non-classically damped structures

A modified modal decomposition method for non-classically damped structures is summarized here. The modal participation factor for damped modes was proposed by Igusa et al.[17] Empirical formulas about relationships between the complex eigenvector Ψ_j and its conjugate pair $\hat{\Psi}_j$ and the damped modal shape ϕ_j and its conjugate pair $\hat{\phi}_j$ are derived as

$$\hat{\Psi}_j = \begin{bmatrix} \lambda_j \boldsymbol{m}\boldsymbol{k}^{-1}\hat{\phi}_j \\ \hat{\phi}_j \end{bmatrix}, \tag{A1}$$

$$\phi_j = \boldsymbol{k}^{-1}\hat{\phi}_j, \tag{A2}$$

where $\boldsymbol{m}$ is the mass matrix, $\boldsymbol{k}$ is the stiffness matrix, and λ_j is the complex eigenvalue of the jth mode. Then, it immediately follows that

$$\Psi_j\hat{\Psi}_j = \phi_j{}^T\left(\boldsymbol{k} - \lambda_j^2\boldsymbol{m}\right)\phi_j, \tag{A3}$$

and it would be $\Psi_j\hat{\Psi}_j = \left(\omega_j^2 - \lambda_j^2\right)\phi_j{}^T\boldsymbol{m}\phi_j$ if the structure is classically damped. The modal mass and modal participation factor for damped modes can be generalized as

$$\hat{m}_j = \frac{\Psi_j \hat{\Psi}_j}{\left(\omega_j^2 - \lambda_j^2\right)}, \tag{A4}$$

$$\gamma_j = \left(\omega_j^2 - \lambda_j^2\right) \frac{{\phi_j}^T \boldsymbol{m}\{e\}}{{\phi_j}^T \left(\boldsymbol{k} - \lambda_j^2 \boldsymbol{m}\right) \phi_j}, \tag{A5}$$

where ω_j is the natural frequency of the jth mode and $\{e\}$ is the unit vector. Note that, if the structure is classically damped, the modal mass and modal participation factor described here would coincide with those for undamped modes.

The modal combination rule for calculation of the maximum acceleration, displacement, shear force and bending moment in the sway direction at the kth node were also proposed by Igusa et al,[17] and they are represented by Equations (A6) to (A9), respectively:

$$A_k = \sqrt{\sum_{j=1}^{m} A_{kj}^2}, \text{with } A_{kj}^2 = \sum_{l=1}^{m} \left[\rho_{jl} \mathrm{Re}\left(\gamma_j \phi_{kj} \nu_j\right) \mathrm{Re}\left(\gamma_l \phi_{kl} \nu_l\right) + \rho'_{jl} \mathrm{Im}\left(\gamma_j \phi_{kj}\right) \mathrm{Im}\left(\gamma_l \phi_{kl}\right)\right] S_a\left(T_j, \zeta_j\right) S_a\left(T_l, \zeta_l\right), \tag{A6}$$

$$D_k = \sqrt{\sum_{j=1}^{m} D_{kj}^2}, \text{with } D_{kj}^2 = \sum_{l=1}^{m} \left[\rho_{jl} \mathrm{Re}\left(\gamma_j \phi_{kj} \nu_j\right) \mathrm{Re}\left(\gamma_l \phi_{kl} \nu_l\right) + \rho'_{jl} \mathrm{Im}\left(\gamma_j \phi_{kj}\right) \mathrm{Im}\left(\gamma_l \phi_{kl}\right)\right] S_a\left(T_j, \zeta_j\right) \left(\frac{T_j}{2\pi}\right)^2 S_a\left(T_l, \zeta_l\right) \left(\frac{T_l}{2\pi}\right)^2, \tag{A7}$$

$$Q_k = \sqrt{\sum_{j=1}^{m} Q_{kj}^2}, \text{with } Q_{kj}^2 = \sum_{l=1}^{m} \left[\rho_{jl} \left\{\sum_{k=i}^{n} \mathrm{Re}\left(\gamma_j \phi_{kj} \nu_j\right) m_k\right\} \left\{\sum_{k=i}^{n} \mathrm{Re}\left(\gamma_l \phi_{kl} \nu_l\right) m_k\right\} + \rho'_{jl} \left\{\sum_{k=i}^{n} \mathrm{Im}\left(\gamma_j \phi_{kj}\right) m_k\right\} \left\{\sum_{k=i}^{n} \mathrm{Im}\left(\gamma_l \phi_{kl}\right) m_k\right\}\right] S_a\left(T_j, \zeta_j\right) S_a\left(T_l, \zeta_l\right), \tag{A8}$$

$$M_k = \sqrt{\sum_{j=1}^{m} M_{kj}^2}, \text{with } M_{kj}^2 = \sum_{l=1}^{m} \left[\rho_{jl} \left\{\sum_{k=i}^{n} \mathrm{Re}\left(\gamma_j \phi_{kj} \nu_j\right) m_k \left(z_n - z_k\right)\right\} \left\{\sum_{k=i}^{n} \mathrm{Re}\left(\gamma_l \phi_{kl} \nu_l\right) m_k \left(z_n - z_k\right)\right\} + \rho'_{jl} \left\{\sum_{k=i}^{n} \mathrm{Im}\left(\gamma_j \phi_{kj}\right) m_k \left(z_n - z_k\right)\right\} \left\{\sum_{k=i}^{n} \mathrm{Im}\left(\gamma_l \phi_{kl}\right) m_k \left(z_n - z_k\right)\right\}\right] S_a\left(T_j, \zeta_j\right) S_a\left(T_l, \zeta_l\right), \tag{A9}$$

where ϕ_{kj} is the damped modal shape of the jth mode at the kth node, $S_a(T_j, \zeta_j)$ is the acceleration response spectrum of the jth mode corresponding to its natural period T_j and modal damping ratio ζ_j, m_k is the kth nodal mass, m and n are the highest mode and node considered for calculations, z_n and z_k are the nth and kth nodal heights, ρ_{jl} and ρ'_{jl} are correlation coefficients between the jth and lth modes, and ν_j is the non-dimensional parameter. The correlation coefficient ρ_{jl} is represented as Equation (13), and ρ'_{jl} is expressed as

$$\rho'_{jl} = \frac{1}{\sqrt{\left(1 - \zeta_j^2\right)\left(1 - \zeta_l^2\right)}} \frac{\zeta_l + r_{jl}\zeta_j}{\zeta_j + r_{jl}\zeta_l} \rho_{jl}, \nu_j = 1 - \frac{\zeta_j}{\sqrt{1 - \zeta_j^2}} i, \tag{A10}$$

where $r_{jl} = \omega_l / \omega_j$ is the natural frequency ratio of the jth to lth modes and ν_j is the non-dimensional parameter.

However, Equations (A6) to (A9) may cause a large error in the predicted seismic responses due to empirical assumptions in the definition of the modal participation factor as Equation (A5) and no consideration of the correlation between components of Ψ_j in the modal combination rule, as shown by Zhou et al.[38]

On the other hand, Figure A1 shows vertical profiles of the real and imaginary parts of damped modal shapes ϕ_j of the 2-MW wind turbine on the soil type II. Imaginary parts of damped modal shapes, which are corresponding to the sway mode of towers (the first, second, fourth, and fifth modes), are negligible due to the low structural damping ratio of wind turbines. Therefore, the modal participation factor can be expressed by the same form as that for undamped modes as Equation (3).

$$\gamma_j = \frac{{\phi_j}^T \boldsymbol{m}\{e\}}{{\phi_j}^T \boldsymbol{m} \phi_j}. \tag{A11}$$

Equation (A11) is used as the modal participation factor for damped modes in Section 3.2, and seismic loadings on towers can be accurately estimated. Nevertheless, it should be noted that seismic loadings on footings might be underestimated using this equation because the imaginary part of the damped modal shape corresponding to the sway motion of foundations (the third mode on the soil type II) is not negligible due to the large modal damping ratio of this mode.

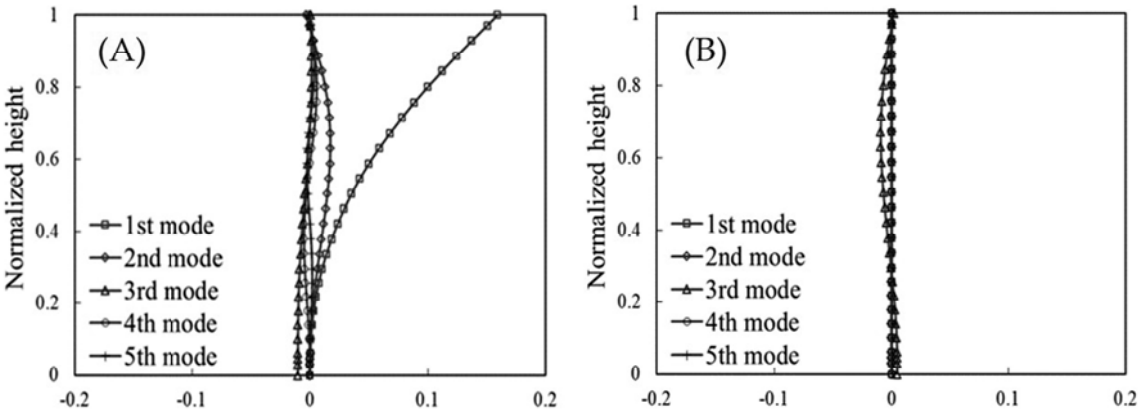

FIGURE A1 Damped modal shapes on the soil type II: (A) real part and (B) imaginary part